Macedonian Journal of Chemistry and Chemical Engineering, Vol. **45**, No. 1, pp. 75–90 (2026)

MJCCA9 – 934

ISSN 1857-5552
e-ISSN 1857-5625

Received: August 19, 2025
Accepted: February 4, 2026

DOI: 10.20450/mjcce.2026.3247
Original scientific paper

ENHANCING TiO_2 PHOTOCATALYTIC EFFICIENCY THROUGH THE SYNERGISTIC EFFECT OF TITANIA/CERIA BINARY OXIDE AND SILVER DOPING

Marija B. Vasić Jovev[1*], Aleksandra B. Krstić[1], Marjan S. Randjelović[1], Radomir B. Ljupković[1], Katarina D. Stepić[1], Miloš M. Marinković[2], Aleksandra R. Zarubica[1*]

[1]*University of Niš, Faculty of Sciences and Mathematics, Department of Chemistry, Višegradska 33, 18000 Niš, Serbia*
[2]*University of Belgrade, Institute of General and Physical Chemistry, Studentski trg 12/V, P.O. Box 45, 11158 Belgrade, Serbia*
marija.vasic@pmf.edu.rs, zarubica2000@yahoo.com

In this study, a modified sol–gel method was used to synthesize pure TiO_2 and TiO_2/CeO_2-based materials, followed by the loading of 3 wt.% silver ions onto the catalyst surfaces using a wet-impregnation method. All synthesized and modified catalysts were characterized using Brunauer–Emmett–Teller (BET), scanning electron microscopy (SEM), and X-ray diffraction (XRD) techniques to analyze their textural, morphological, and structural properties. The photocatalytic activity of these materials was evaluated for the degradation/decolorization of crystal violet (CV) dye under ultraviolet (UV) irradiation. Moreover, the effects of various process parameters, including initial dye concentration, catalyst amount, and UV wavelength, on photocatalytic efficiency were analyzed. The results indicated that the addition of CeO_2 and Ag into the TiO_2 catalyst significantly enhanced the photocatalytic activity compared with pure TiO_2 under identical experimental conditions. Further analysis of the photocatalytic process demonstrated that the TiO_2/CeO_2 binary oxide catalyst, as well as Ag-doped samples (TiO_2/Ag and TiO_2/CeO_2/Ag), exhibited improved photocatalytic performance relative to pure TiO_2.

Keywords*:* titania; ceria; Ag-doping; photocatalysis

ПОДОБРУВАЊЕ НА ФОТОКАТАЛИТИЧКАТА ЕФИКАСНОСТ НА TiO_2 ПРЕКУ СИНЕРГЕТСКИОТ ЕФЕКТ НА БИНАРЕН ТИТАНИУМ/ЦЕРИУМ ДИОКСИД И ДОПИНГУВАЊЕ СО СРЕБРО

Во оваа студија беше применет модифициран сол–гел-метод за синтеза на чист TiO_2 и материјали базирани на TiO_2/CeO_2, по што беше извршено нанесување на 3 % сребрени јони на површината на катализаторите со методот на влажна импрегнација. Сите синтетизирани и модифицирани катализатори беа карактеризирани со примена на техниките Brunauer–Emmett–Teller (BET), скенирачка електронска микроскопија (SEM) и рендгенска дифракција (XRD), со цел да се анализира нивната текстура, како и морфолошки и структурни својства.

Фотокаталитичката активност на овие материјали беше испитувана преку деградација/деколоризација на бојата кристално виолетово (CV) под ултравиолетово (UV) зрачење. Дополнително беше анализирано и влијанието на различни процесни параметри врз фотокаталитичката ефикасност, вклучувајќи ги почетната концентрација на бојата, количината на катализаторот и брановата должина на UV-зрачењето.

Резултатите покажаа дека додавањето на CeO_2 и Ag во TiO_2-катализаторот значително ја зголемува фотокаталитичката активност во споредба со чистиот TiO_2 при исти експериментални услови. Понатамошната анализа на фотокаталитичкиот процес покажа дека бинарниот оксиден катализатор TiO_2/CeO_2, како и примероците допингувани со Ag (TiO_2/Ag и TiO_2/CeO_2/Ag), покажуваат подобрени фотокаталитички перформанси во однос на чистиот TiO_2.

Клучни зборови: титаниум диоксид; цериум диоксид; допингување со Ag; фотокатализа

1. INTRODUCTION

In recent years, titanium dioxide (TiO_2) has gained significant attention due to its high efficiency and favorable characteristics, including cost-effectiveness, thermal stability, and chemical stability.[1,2] These advantageous properties have resulted in extensive research, particularly on the photocatalytic degradation of organic pollutants, pigment applications, and gas-sensing technologies.[1,3–6] TiO_2 has been widely investigated for water and air purification due to its excellent photocatalytic properties.[1,3] Reactive organic dyes, originating from various industrial activities and capable of entering waters, pose a significant environmental threat. Consequently, this issue has become a major concern for scientists. One such hazardous dye is crystal violet, which is toxic, exhibits mutagenic properties, and poses risks to a wide range of aquatic organisms.[7,8] Conventional methods for the removal of organic pollutants often suffer from certain limitations or require prolonged treatment times, and their effectiveness depends on pollutant characteristics and operating conditions.[9,10] Recent scientific advancements have driven the development of numerous alternative purification methods, among which heterogeneous photocatalysis has emerged as a particularly notable approach.[11,12]

TiO_2 occurs in three main polymorphic phases: rutile, anatase, and brookite.[13] Its photocatalytic activity is primarily derived from its semiconducting and photosensitive behavior. Although titania is an excellent photocatalyst, its major limitations include a wide band gap and rapid electron–hole (e^-/h^+) recombination. Due to the wide band gap of the pure anatase phase (approximately 3.2 eV), UV irradiation is required to initiate photoexcitation in photon-driven applications of titania.[3,13] To overcome these limitations, researchers have extensively investigated methods for band-gap reduction, particularly through doping with metal ions, which can modify the surface properties and induce crystal defects, thereby significantly enhancing photocatalytic properties.[3,14]

To improve the photocatalytic activity of pristine TiO_2, surface modification and doping with noble metals, such as silver (Ag), gold (Au), and platinum (Pt), have been widely investigated.[15–18] Furthermore, numerous studies have demonstrated that the incorporation of rare earth metal ions can substantially enhance the photocatalytic performance of TiO_2. In particular, the incorporation of cerium ions, which possess 4f electrons, into the TiO_2 lattice has been shown to suppress electron–hole recombination, thereby significantly enhancing photocatalytic activity.[3,19,20]

Ceria (CeO_2) exhibits characteristic optical properties, including strong UV absorption, which is attributed to its band gap of approximately 3.2 eV.[20] The electronic transitions between the valence and conduction bands of CeO_2 account for this UV absorption behavior.[3,19,20] Additionally, the ability of cerium (Ce) to exist in both Ce^{3+} and Ce^{4+} oxidation states contributes to its unique redox behavior and catalytic activity. In summary, the coexistence of Ce^{3+}/Ce^{4+} redox couples, together with high oxygen storage capacity, contributes to the strong catalytic potential of ceria.[19,20] The mentioned doping and modification processes can extend the light absorption range of titania, thereby improving its effectiveness in harnessing visible light.[3,20]

It is well known that the synthesis method and experimental conditions significantly influence the physicochemical properties and photocatalytic activity of TiO_2-based catalysts.[21–23] Therefore, the careful selection of synthesis method and preparation conditions is crucial for achieving the desired properties of the final material.[21] Numerous methods have been used for the preparation of titania-based materials, including sol–gel, hydrothermal, solvothermal, and microwave-assisted techniques, among others,[21,24–26] with sol–gel and hydrothermal methods being the most widely used.[21,24]

The sol–gel method is a relatively simple method for preparing homogeneous, high-purity materials.[21,27] Moreover, it does not require expensive equipment or harsh reaction conditions and can be conducted at ambient temperature and atmospheric pressure.[21] However, calcination is a necessary step in the sol–gel method for obtaining a crystalline TiO_2 structure. The calcination temperature determines the crystal phase composition, as well as the structural, morphological, and other physicochemical properties of the final material, and consequently its photocatalytic activity.[28,29]

In this paper, we present the synthesis of TiO_2 and Ag-doped TiO_2 (TiO_2/Ag) catalysts prepared using a modified sol–gel method. Additionally, TiO_2/CeO_2 and Ag-doped TiO_2/CeO_2 (TiO_2/CeO_2/Ag) catalysts were successfully synthesized via the sol–gel method. The calcination temperature employed in this study was 550 °C, chosen to obtain titania with a highly active anatase phase and/or mixed anatase–rutile phases, thereby achieving optimal crystallinity and crystallite size, which are important for photocatalytic activity.[28,29]

This research primarily focuses on the synthesis of modified titania, examining the effects of silver-ion impregnation on the physicochemical properties of TiO_2 and TiO_2/CeO_2 catalysts, and evaluating their photocatalytic activity in the decolorization/degradation of the cationic dye crystal violet. Furthermore, the study investigates the influence of key process parameters on photocatalytic efficiency, including catalyst loading, initial dye concentration, and UV irradiation wavelength.

To the best of our knowledge, no studies have been reported in the scientific literature that describe an identical preparation method for Ag-doped TiO_2/CeO_2 catalysts, utilizing the same composition ratios, precursor materials, and synthesis conditions, and evaluated for the photocatalytic degradation of the organic dye crystal violet under identical experimental conditions. Therefore, this work is considered novel, as it includes these specific synthesis and testing parameters and provides new insights into the photocatalytic behavior and performance of the resulting materials.

2. EXPERIMENTAL SECTION

2.1. *Materials*

All chemicals used in this study, including titanium(IV) isopropoxide ($Ti[OCH(CH_3)_2]_4$, Sigma Aldrich), 2-propanol ($(CH_3)_2CHOH$, Sigma Aldrich), silver nitrate ($AgNO_3$, Sigma Aldrich), cerium(III) nitrate hexahydrate ($Ce(NO_3)_3{\cdot}6H_2O$, Sigma Aldrich), and crystal violet ($C_{25}H_{30}N_3Cl$, Merck), were of analytical grade and used without additional purification.

The chemical structure of crystal violet dye is shown in Figure 1.[7,30]

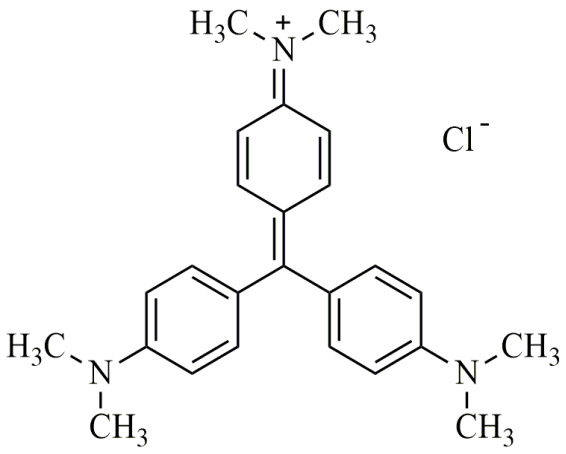

Fig. 1. Chemical structure of crystal violet dye

2.2. *Synthesis of TiO_2*

A TiO_2-based catalyst was synthesized using a modified sol–gel method. The initial step involved the preparation of two solutions. The first solution was prepared by dissolving a calculated amount of titanium(IV) isopropoxide in 2-propanol. The second solution was prepared by mixing 2-propanol and water in a volume ratio of 1:4, which was added dropwise to the first solution under vigorous stirring for 1 h. The process of combining these two solutions was carried out under a nitrogen atmosphere.

The pH of the resulting suspension was adjusted to 9 by the addition of NH_4OH. The formed precipitate was separated by filtration, washed with distilled water, and then rinsed with a mixture of isopropanol and water. The resulting powder sample was dried at 105 – 110 °C for 3 h. A portion of the prepared material was subsequently calcined at 550 °C for 3 h, using a heating rate of 10 °C/min, resulting in a pure TiO_2 catalyst, hereafter denoted as T. The remaining portion was reserved for subsequent doping procedure.

2.3. *Synthesis of TiO_2/Ag*

The Ag-doped TiO_2 (TiO_2/Ag) sample, hereinafter denoted as TA, was prepared by incorporating 3 wt.% Ag into a portion of pristine TiO_2 obtained in the previous step, using the wet impregnation method. The TiO_2 powder was accurately weighed and placed in a rotary vacuum evaporator, to which a calculated amount of $AgNO_3$ dissolved in distilled water was added. The resulting suspension was continuously stirred in the rotary vacuum evaporator until the solvent was completely removed. Subsequently, the impregnated material was dried at 60 – 65 °C for 3 h. The doped catalyst was then calcined at 550 °C for 3 h, using a heating rate of 10 °C/min.

2.4. *Synthesis of TiO_2/CeO_2*

The CeO_2/TiO_2 binary oxide was successfully synthesized via the sol–gel method. The initial solution was prepared by dissolving a precise amount of titanium(IV) isopropoxide in 2-propanol. A second solution was prepared by mixing 2-propanol and water in a 1:4 volume ratio. The second solution was added slowly to the first, and the resulting mixture was vigorously stirred for 1 h under a nitrogen atmosphere. Subsequently, a hydrogen peroxide solution was added dropwise

under continuous stirring, causing the pH to decrease to 4.5.

In parallel, the $Ce(NO_3)_3$ solution was prepared by dissolving an appropriate amount of cerium(III) nitrate hexahydrate in distilled water. The entire volume of the prepared $Ce(NO_3)_3$ solution was added dropwise to the previously prepared suspension. The TiO_2/CeO_2 binary oxide was obtained by adding 10 wt.% of $Ce(NO_3)_3$. The pH of the resulting suspension was then adjusted to 9 by the addition of NH_4OH. The formed precipitate was filtered, rinsed with distilled water, and then washed with a mixture of isopropanol and water.

The resulting powder sample was dried at 105 – 110 °C for 3 h, and a portion of the prepared material subsequently calcined at 550 °C for 3 h, using a heating rate of 10 °C/min. This process resulted in obtaining the TiO_2/CeO_2 sample, hereinafter denoted as TC. The remaining portion of the material was reserved for the preparation of the Ag-doped sample ($TiO_2/CeO_2/Ag$).

2.5. *Synthesis of modified $TiO_2/CeO_2/Ag$*

The Ag-doped TiO_2/CeO_2 catalyst ($TiO_2/CeO_2/Ag$), hereinafter denoted as TCA, was obtained by incorporating 3% Ag, relative to the mass of the base catalyst, using the same procedure as that described for the TA sample.

2.6. *Catalyst characterization*

Brunauer–Emmett–Teller (BET) surface area measurements were carried out via N_2 adsorption–desorption using a Micromeritics ASAP 2010, with He as the carrier gas. X-ray diffraction (XRD) was employed to investigate the structural characteristics of the catalysts. XRD patterns were recorded using a Philips APD-1700 diffractometer equipped with a Cu anticathode, operating at 40 kV and 55 mA. The crystalline size was estimated using the Scherrer Equation (1):[3,31,32]

$$D = \frac{K\lambda}{\beta \cos\theta} \quad (1),$$

where D is the crystallite size, K is the Scherrer constant, λ is the X-ray wavelength, β is the full width at half maximum of the corresponding peaks (the (101) peak for anatase and the (110) peak for rutile), and θ is the Bragg angle.[3,31,32]

The weight fraction of the rutile phase was calculated using Equation (2):[3,33,34]

$$X_R = \frac{1}{1 + 0.8 \times \frac{I_A}{I_R}} \quad (2),$$

where X_R represents the weight fraction of the rutile crystal phase, and I_A and I_R denote the integrated XRD intensities of the (101) reflection of the anatase and the (110) reflection of the rutile phase, respectively.[3,33,34]

The surface morphology of the prepared catalysts was examined by scanning electron microscopy (SEM) using a JEOL JSM-6460LV scanning electron microscope.

2.7. *Photocatalytic activity*

The photocatalytic activity of the catalysts was evaluated by investigating the degradation of crystal violet (CV) dye under UV lamp irradiation (Roth Co., 16 W, 2.5 mW/cm^2, with a maximum emission at 254 nm, unless otherwise stated). The UV lamp was positioned 10 cm from the reaction mixture containing the catalyst and CV dye solution, which was continuously stirred on a magnetic stirrer. The initial pH of the CV dye solution ranged from 6.7 to 7.0 and was not adjusted prior to the photocatalytic experiments.

Before UV irradiation, the catalysts were mixed in a CV test solution and stirred continuously in the dark for 24 h. This mixture was then maintained in the dark for an additional 12 h to ensure that the adsorption–desorption equilibrium was achieved. Approximately 31 – 38% of the CV dye was adsorbed on the catalyst surfaces after 24 h. After the adsorption–desorption equilibrium was established, the catalyst was separated, and a fresh CV dye solution was introduced before the photocatalytic reaction was conducted.

To analyze the CV dye degradation/decolorization process, the absorbance was measured at its maximum wavelength (λ_{max} = 590 nm), using a UV–Vis spectrophotometer (Shimadzu Co.). Aliquots were withdrawn at specified time intervals, centrifuged, filtered, and subsequently analyzed for their absorbance values. The photocatalytic efficiency, defined as the percentage of dye removal, was calculated using Equation (3):[35]

$$\text{Photocatalytic efficiency (\%)} = \left(1 - \frac{C_t}{C_0}\right) \times 100 \quad (3)$$

where C_t is the CV dye concentration at a specific time t (mmol/dm^3), and C_0 represents the initial CV dye concentration (mmol/dm^3).

Moreover, the process parameters that were varied during the photocatalytic performance tests included catalyst loading, initial CV dye concentration, and the wavelength of the applied UV irradiation.

3. RESULTS AND DISCUSSION

3.1. *Textural characterization*

The textural characteristics of the prepared samples, namely pristine TiO_2 (T), TiO_2/Ag (TA), TiO_2/CeO_2 (TC), and TiO_2/CeO_2/Ag (TCA), are presented in Table 1.

Table 1

Textural characteristics (specific surface area, average pore diameter, and pore volume) of the prepared samples TiO_2, TiO_2/Ag, TiO_2/CeO_2, and TiO_2/CeO_2/Ag

Sample	S_{BET} (m^2g^{-1})	d_P (nm)	V_P (cm^3g^{-1})
T	7.747	96.42	0.0424
TA	4.119	147.19	0.0589
TC	80.303	7.94	0.1364
TCA	55.326	8.14	0.1190

The BET surface area of the T sample was estimated to be 7.75 m^2/g, which was significantly lower than the values reported by other authors.[36] After modification of the TiO_2-based material with Ag, sample TA exhibited a decreased specific surface area and an increased mean pore diameter. This behavior was attributed to the insufficient and/or non-uniform dispersion of silver (Ag^+) ions on the catalyst surface.[10] Moreover, the observed reduction in BET surface area and porosity could also be ascribed to enhanced particle agglomeration, as discussed later in the SEM analysis. While these textural characteristics may influence the photocatalytic performance of the synthesized samples, they were not considered decisive factors for their overall efficiency. Namely, it has been reported in the literature that the presence of Ag can enhance photocatalytic activity.[37]

The synthesized TC sample exhibited a significantly higher specific surface area, a smaller average pore diameter, and a larger pore volume compared with pristine TiO_2. The obtained textural characteristics of the prepared TC material were comparable with values reported by other authors.[36]

After Ag doping of the TC sample, the resulting TCA sample was characterized with optimal textural properties, including favorable specific surface area, mean pore diameter, and pore volume. These enhanced characteristics were expected to facilitate the adsorption of organic pollutants on the catalyst surface, thereby promoting improved photocatalytic performance. The textural properties of the prepared samples (T, TA, TC, and TCA), along with their nitrogen adsorption–desorption isotherms and pore size distribution curves (insets), are presented in Figure 2.

The results presented in Figures 2a and 2b demonstrated that pure T and TA samples exhibited type III adsorption isotherms with an H3 hysteresis loop, according to the IUPAC classification.[38–40] This type of hysteresis loop is commonly associated with the formation of aggregates composed of plate-like particles, resulting in slit-shaped pores.[38,39,41] Type III isotherms are characteristic of macroporous and/or nonporous materials,[38,42] which was consistent with the mean pore diameter values presented in Table 1 for T and TA.

The pore size distribution results showed that both materials exhibited multimodal pore size distribution (Fig. 2a, b, insets). As shown in Figure 2a (inset), the pristine TiO_2-based catalyst was characterized by the presence of micropores with a mean pore diameter of approximately 2.5 nm, macropores with a mean pore diameter of 60 nm, and a significant volume of macropores with a mean pore diameter of approximately 100 nm. As mentioned, the TA sample also displayed a multimodal pore distribution (Fig. 2b, inset), containing boundary micro-mesopores with a mean diameter of approximately 3 nm, mesopores around 40 nm, macropores of approximately 80 nm, and larger pores in the 100 – 200 nm range.[42]

The nitrogen adsorption–desorption isotherms further indicated that both T (Fig. 2a) and TA (Fig. 2b) samples exhibited very narrow hysteresis loops within the relative pressure (p/p_0) range of 0.8 – 0.9. Consequently, these materials were characterized by a larger volume of macropores and a smaller amount of mesopores, which was further supported by the pore size distribution results presented in the insets of Figures 2a and 2b.[40,41,43]

The samples TC and TCA were characterized by type IV isotherms with an H2 hysteresis loop (Fig. 2c, d).[38] These features are associated with a broad distribution of pore sizes and shapes, forming interconnected pore networks.[38–41,43] Such materials exhibited a complex pore structure and were commonly described as possessing ink-bottle-shaped pores.[40,41,43] Furthermore, type IV isotherms are typically associated with capillary condensation occurring in mesopores.[41] The H2 hysteresis loop, attributed to capillary condensation, is often linked to ink-bottle-type pores and indicative of pore network effects or pore blocking, reflecting a nonuniform pore structure.[40,44]

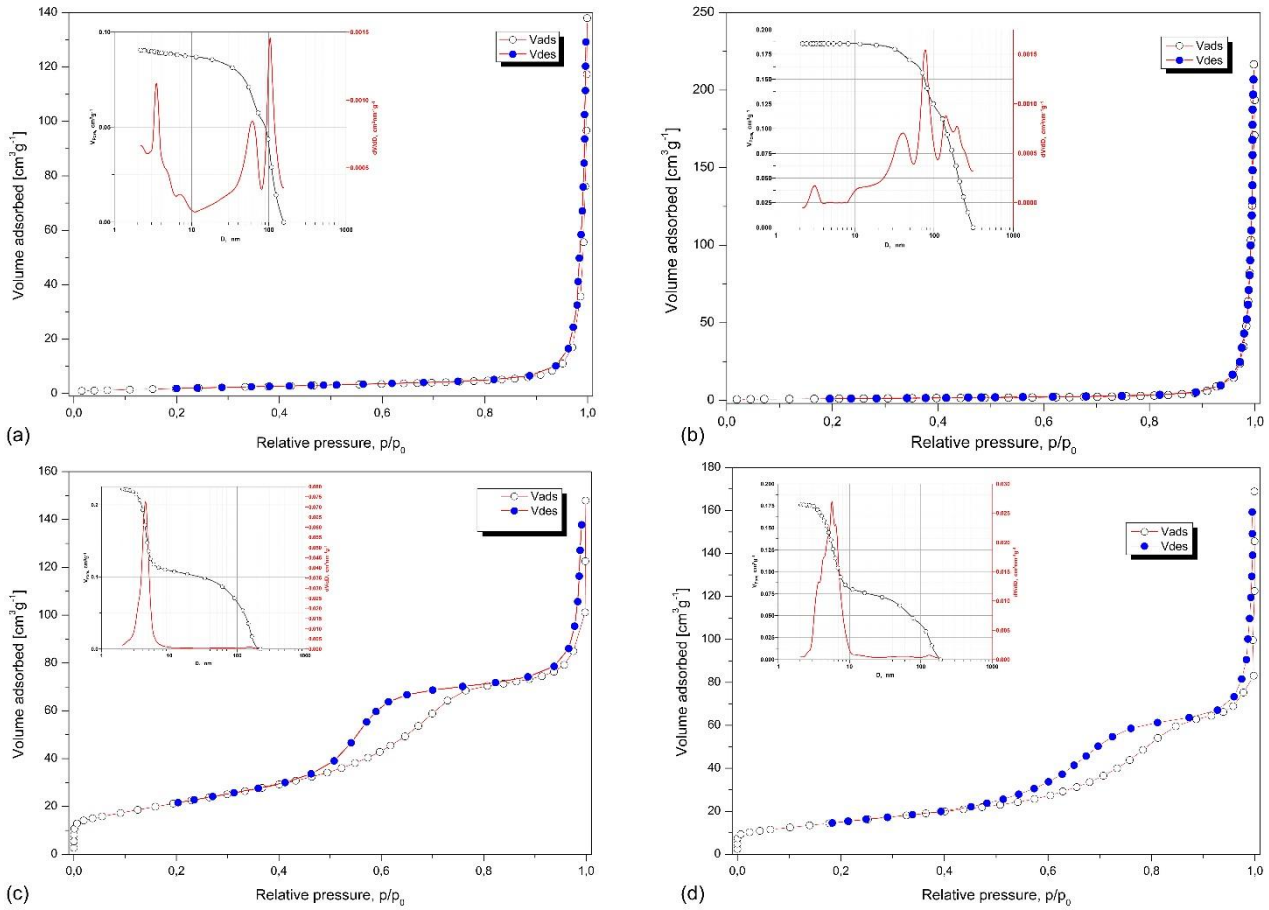

Fig. 2. Nitrogen adsorption–desorption isotherms and pore size distribution curves (insets) of: (a) TiO_2, (b) TiO_2/Ag, (c) TiO_2/CeO_2, and (d) TiO_2/CeO_2/Ag samples

Interestingly, this interpretation did not fully correlate with the pore size distribution results obtained for the TC sample (Fig. 2c, inset). Analysis of the TC pore size distribution revealed a uniform pore structure, consisting exclusively of mesopores with a mean pore diameter of 4.5 nm, corresponding to a monomodal pore distribution. This behavior is more commonly associated with the H1 hysteresis type described in the literature.[38,40] The H1 hysteresis loop is typically characterized by porous materials composed of agglomerates, nearly uniform spherical particles, leading to cylindrical pore shapes and a narrow pore size distribution.[38,40] However, the TC sample did not exhibit behavior fully consistent with the H1 hysteresis type,[40] but instead displayed features characteristic of an H2 hysteresis loop.

Nevertheless, the pore size distribution of the TCA sample (Fig. 2d) revealed predominantly mesoporous characteristics, with a slightly nonuniform yet relatively narrow pore size distribution, centered at a dominant pore diameter of approximately 6 nm. This behavior was consistent with a non-typical H2-type hysteresis loop.[40] Furthermore, the isotherms and hysteresis loops of both TC (Fig. 2c) and TCA (Fig. 2d) samples were broad and steep.

The isotherms for the TCA sample were shifted downward and toward lower relative pressures, within the p/p_0 range of approximately 0.4 – 0.8, compared with the TC sample. Adsorption occurring in the relative pressure of p/p_0 = 0.4 – 0.9 was indicative of capillary condensation within mesopores, resulting in a hysteresis loop in which the desorption branch was positioned above the adsorption curve.[44] Consequently, these materials were characterized by a higher proportion of mesopores, as confirmed in the insets of Figs. 2c and 2d. These observations were consistent with those described in the scientific literature.[40,41,43,44]

3.2. *Structural characterization*

The XRD patterns of the prepared T, TA, TC, and TCA samples are shown in Figure 3.

X-ray diffraction analysis of all prepared samples indicated the presence of characteristic diffraction peaks corresponding to anatase (101) at approximately 2θ = 25.3° (JCPDS Card No. 21-

1272[31,45,46]) and rutile (110)[3] at approximately 2θ = 27.6° (JCPDS Card No. 21-1276[46]), present in different phase proportions (Fig. 3). The calculated crystallite sizes and the relative contents of anatase and rutile are summarized in Table 2.

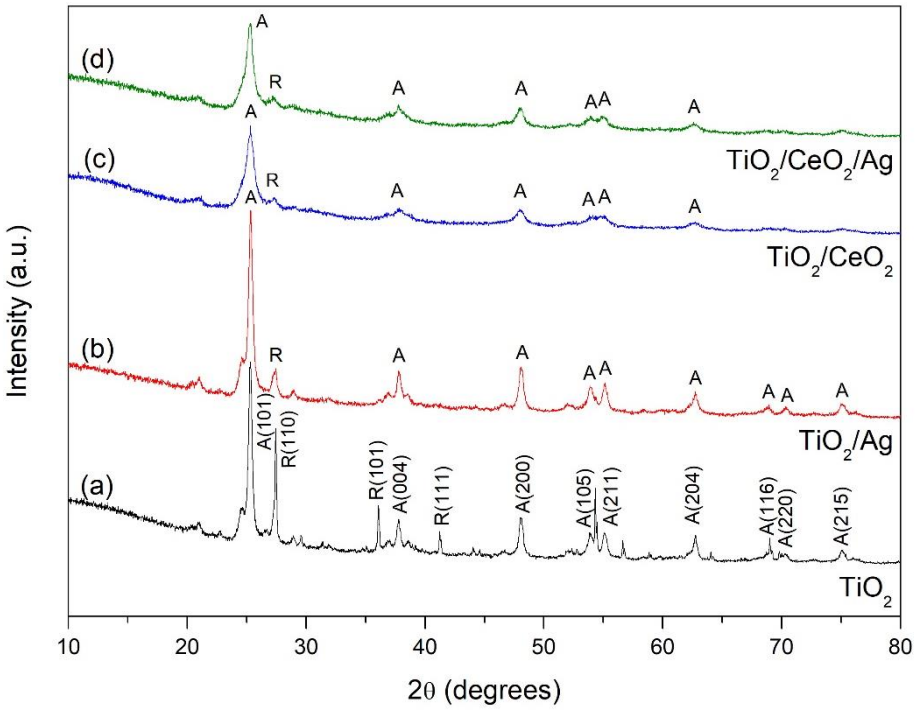

Fig. 3. X-ray diffractograms of: (a) TiO_2, (b) TiO_2/Ag, (c) TiO_2/CeO_2, and (d) TiO_2/CeO_2/Ag

T a b l e 2

Structural properties of TiO_2, TiO_2/Ag, TiO_2/CeO_2, and TiO_2/CeO_2/Ag samples (anatase and rutile crystallite sizes and volume ratios)

Sample	d_A (nm)	d_R (nm)	X_A (%)	X_R (%)
T	21.76	117.47	56.75	43.25
TA	19.97	45.31	87.31	12.69
TC	9.58	30.58	88.37	11.63
TCA	11.96	31.07	93.83	6.17

All modified samples exhibited smaller crystallite sizes compared with pristine TiO_2, indicating that modification with CeO_2 and/or Ag inhibited crystallite growth. Furthermore, it was noticeable that these modification processes suppressed the anatase-to-rutile phase transformation (Table 2). Based on the results for pristine TiO_2, it was observed that this sample contained a mixture of anatase and rutile crystal phases (Table 2, Fig. 3a), with an anatase-to-rutile volume ratio of approximately 57:43. This result was slightly different from expectations, considering the calcination temperature of 550 °C applied during synthesis.

After modification with Ag^+ ions (TA sample, Fig. 3b), XRD analysis indicated an increase in intensity of the anatase (101) peak at 25.3°, while the rutile (110) peak at 27.4° decreased, resulting in anatase becoming the dominant phase. This result confirmed that Ag doping reduced the anatase-to-rutile phase transformation. Moreover, Ag incorporation led to the formation of significantly smaller rutile crystallites and with slightly reduced anatase crystallite sizes in the TA sample compared with pristine TiO_2 (Table 2), which could potentially contribute to enhanced photocatalytic activity.

The synthesis of the TiO_2/CeO_2 binary oxide (TC) also suppressed the anatase-to-rutile phase transformation and reduced crystallite sizes for both the anatase and rutile phases (Table 2, Fig. 3c). Consequently, TC was primarily composed of anatase, accounting for approximately 88 % of the anatase crystalline phase (Table 2). However, the TC sample exhibited lower crystallinity compared to pristine TiO_2 and the Ag-modified TA sample (Fig. 3).

Ag doping of the TC material resulted in a further reduction of the anatase-to-rutile transformation. As a result, the TCA sample was charac-

terized by the almost exclusive presence of anatase (Table 2, Fig. 3d), which is widely recognized as the most photocatalytically active TiO_2 phase. Additionally, a slight enhancement in crystallinity was observed for the TCA sample compared with TC (Fig. 3c, d).

Furthermore, considering the obtained crystallite sizes of the anatase and rutile phases in TCA (Table 2), together with its optimal BET surface area, mean pore diameter, and pore volume (Table 1), the results suggested facilitated adsorption of organic pollutants on the catalytic surface. Accordingly, an improvement in photocatalytic activity was expected. Notably, the diffraction peak characteristic of CeO_2 at approximately $2\theta = 28.5°$ (JCPDS Card No. 81-0792[31,47]), was not detected.

3.3. *Morphological characterization*

The micrographs of T, TA, TC, and TCA samples are presented in Fig. 4.

Based on the results presented in Fig. 4a, the morphology of pristine TiO_2 consisted of spherical primary particles on the nanometer scale, with sizes of approximately 60 nm – 100 nm, along with spherical secondary particles. The smaller primary particles tended to form clusters, whereas the secondary agglomerated particles formed larger aggregates, which correlated well with the textural results presented in Table 1, showing a mean pore diameter of approximately 96 nm and a relatively low specific surface area.

The micrographs of the Ag-modified TA sample (Fig. 4b) revealed the presence of small spherical primary particles, together with agglomerated secondary particles and larger aggregates. This morphology suggested a somewhat irregular distribution of Ag^+ ions within the TiO_2 structure. Furthermore, the TA sample exhibited altered porosity compared with pristine TiO_2, as the presence of interparticle pores between agglomerates was more noticeable. These observations, namely the formation of larger agglomerated particles compared with pure TiO_2, were in good correlation with the textural results, which indicated an increase in the mean pore diameter and a decrease in BET surface area compared to pristine TiO_2 (Table 1).

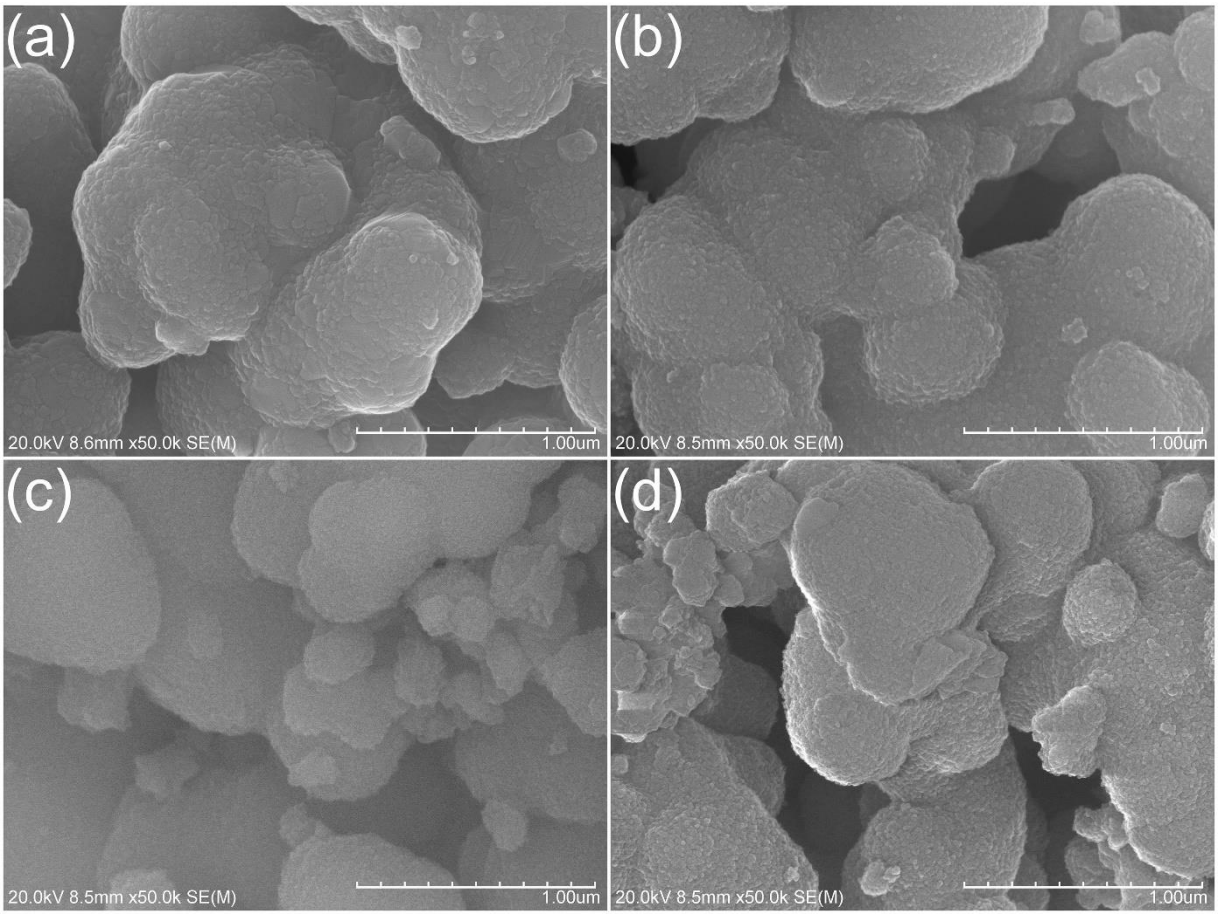

Fig. 4. SEM images of the prepared samples: (a) TiO_2, (b) TiO_2/Ag, (c) TiO_2/CeO_2, and (d) TiO_2/CeO_2/Ag

The synthesis of the TC sample resulted in enhanced porosity and the formation of a larger amount of spherical primary particles (Fig. 4c) compared with pure TiO_2. Although agglomerates remained present, their occurrence was significantly reduced relative to pristine TiO_2. This behavior was consistent with the increase in surface area obtained from BET analysis (Table 1) and corresponded well to the particle sizes estimated from XRD data (Table 2).

The modified TCA sample exhibited a predominantly spherical morphology, with a more uniform distribution of primary particles, having sizes of approximately 50 nm, along with secondary agglomerated particles (Fig. 4d). The morphological changes were consistent with the textural and structural properties determined from BET and XRD analyses (Tables 1 and 2).

3.4. *Photocatalytic activity*

The photocatalytic activity of all prepared samples, T, TA, TC, and TCA, is presented in Fig. 5. All experimental conditions were kept constant for all photocatalytic reactions, with C_0 = 0.005 mmol/dm^3, m = 40 mg, and λ = 254 nm.

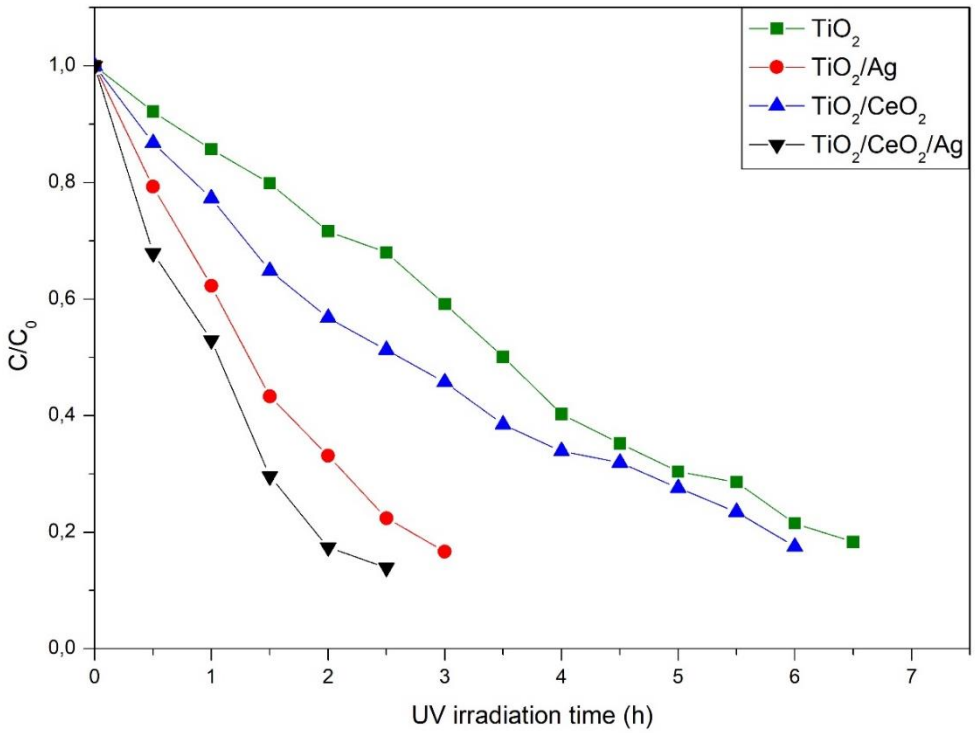

Fig. 5. Effect of the use of different prepared catalysts (TiO_2, TiO_2/Ag, TiO_2/CeO_2, and TiO_2/CeO_2/Ag) on the degradation/decolorization of the crystal violet dye

The results presented in Fig. 5 demonstrated that photocatalytic activity increased in the following order: T < TC < TA < TCA. The TCA sample exhibited the highest photocatalytic activity among the tested materials; after a photocatalytic reaction time of 2.5 h, approximately 86% of the dye was removed (Table 3). This enhanced performance was attributed to its favorable physicochemical properties. The TCA sample exhibited optimized characteristics, including a suitable specific surface area, favorable mean pore diameter and pore volume, appropriate morphology, acceptable crystallinity with optimal crystallite sizes, and an almost exclusive presence of the anatase crystalline phase. Collectively, these properties facilitated the adsorption of organic pollutants, such as the selected CV dye, on the catalyst surface and enhanced the transport of reactants to catalytically active sites during the photocatalytic process.[10]

Although the TA sample had a relatively small specific surface area, it exhibited good photocatalytic activity, indicating that this parameter was not decisive factor determining its performance. The structural characteristics of the TA material showed good crystallinity, acceptable anatase and rutile crystallite sizes, a dominant presence of the most photocatalytically active phase anatase, and adequate porosity. Moreover, it has

been widely reported that surface modifications, such as doping with noble metals (e.g., Ag, Au) can enhance photoinduced charge separation and suppress recombination of e^-/h^+ pairs.[15,17,37] In addition, such modification is often associated with a red shift in the absorption spectrum towards the visible region, accompanied by a reduction in band-gap energy.[15,17,37] These effects can collectively contribute to the improved photocatalytic activity of the TA sample compared with the unmodified TiO_2.

Although the TC sample exhibited a relatively large specific surface area, it was less active than TA, which was attributed to the absence of Ag^+ ions, as discussed earlier. Nevertheless, the TC sample showed enhanced photocatalytic performance compared with pristine TiO_2 (Fig. 5), which was primarily attributed to the suppression of crystallite growth during the modification process, along with favorable textural, structural, and morphological properties. Furthermore, it has been suggested that the formation of TiO_2/CeO_2 mixed oxides can form catalysts with enhanced adsorption capacity and more efficient charge-carrier separation, due to the generation of oxygen vacancies and synergistic interactions between TiO_2 and CeO_2, as reported in the literature.[48-51] These combined factors contributed to the improved photocatalytic activity of the TC sample compared to the pure TiO_2.

3.5. *Influence of the process parameters on the photocatalytic reactions*

3.5.1. *Effect of initial dye concentration*

The effect of different initial CV dye concentrations on the photocatalytic activity of the modified $TiO_2/CeO_2/Ag$ catalyst is presented in Fig. 6. The tested initial concentrations of CV dye were C_{01} = 0.005 mmol/dm^3, C_{02} = 0.0075 mmol/dm^3, and C_{03} = 0.01 mmol/dm^3. All other experimental conditions were kept constant for all reactions.

The results shown in Fig. 6 indicated that, with increasing initial concentration of the tested CV dye solution, the degradation time of the photocatalytic process increased. This behavior was attributed to the greater saturation of catalytically active sites by dye molecules at higher dye concentrations, as well as to reduced UV light penetration resulting from the higher optical density of the dye solution.

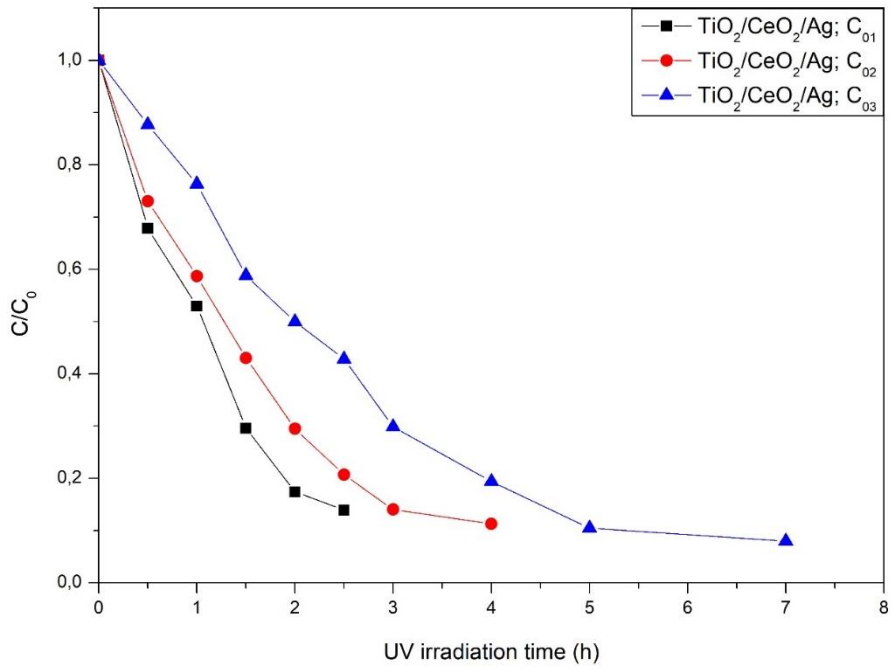

Fig. 6. Influence of initial dye concentration on the photo-degradation of the crystal violet dye using a $TiO_2/CeO_2/Ag$ catalyst

In Figure 7, the effect of the initial CV dye concentration on the photocatalytic efficiency (% dye removal) of all samples after 150 min of photocatalytic reaction, under the same reaction conditions, is presented. All tested samples exhibited higher photocatalytic efficiency with a decrease in the initial dye concentration (Fig. 7, Table 3).

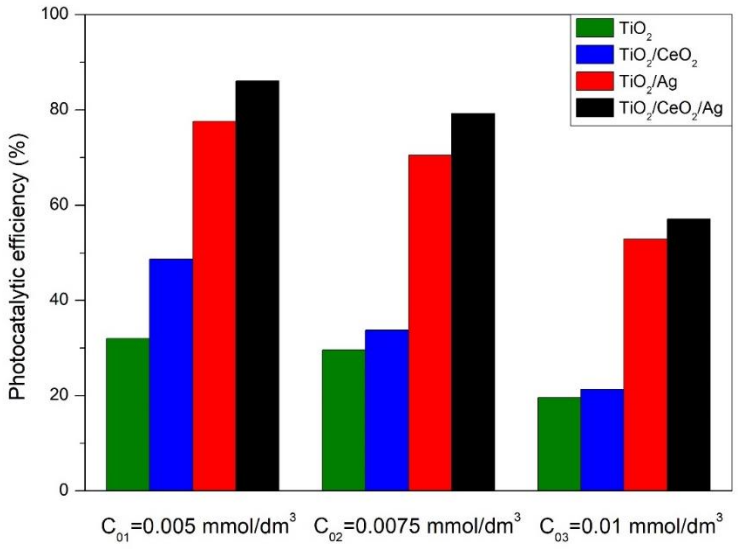

Fig. 7. Influence of the initial crystal violet dye concentration on photocatalytic efficiency (dye removal in %) for the prepared samples: TiO_2, TiO_2/CeO_2, TiO_2/Ag, and $TiO_2/CeO_2/Ag$

3.5.2. *Effect of catalyst amount*

The effect of different loadings of the most active, modified TCA catalyst on the photocatalytic process is presented in Figure 8. The experimental conditions applied during the photocatalytic experiments were kept constant for all reactions, as previously described, except for the catalyst amount, which was varied as follows: m_1 = 40 mg, m_2 = 60 mg, and m_3 = 80 mg.

The results presented in Figure 8 indicated that, with increasing catalyst mass, the degradation/decolorization of the CV dye also increased. This behavior was attributed to the presence of a greater number of catalytically active sites when a larger amount of catalyst was used. Consequently, a higher number of photons capable of initiating photocatalytic reactions was adsorbed, thereby enhancing photocatalytic efficiency. A similar trend was observed for all samples after 150 min under the same reaction conditions applied during the photocatalytic process, as presented in Figure 9.

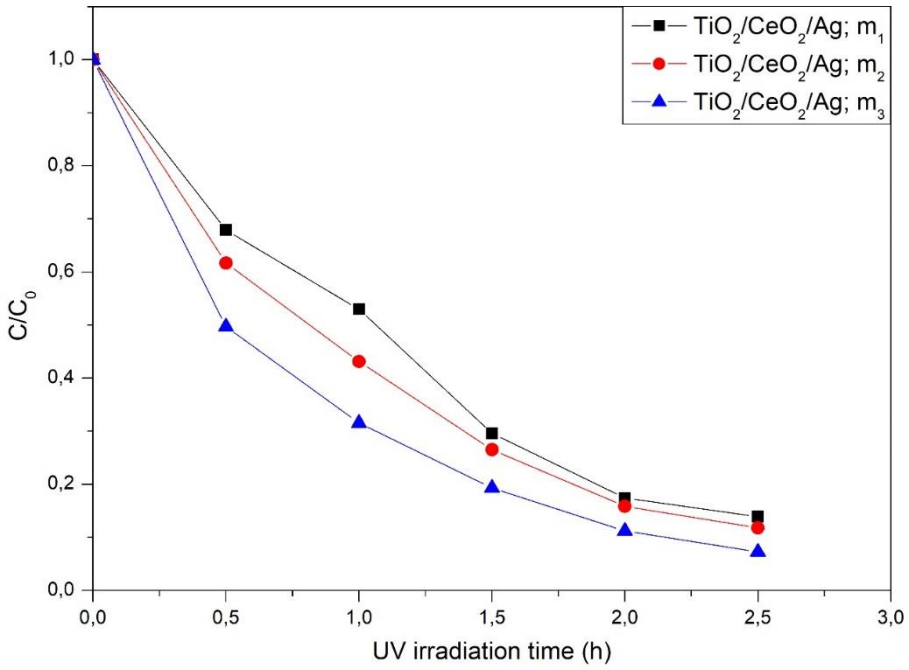

Fig. 8. Effect of catalyst amount on the photo-degradation of the crystal violet dye using a $TiO_2/CeO_2/Ag$ catalyst

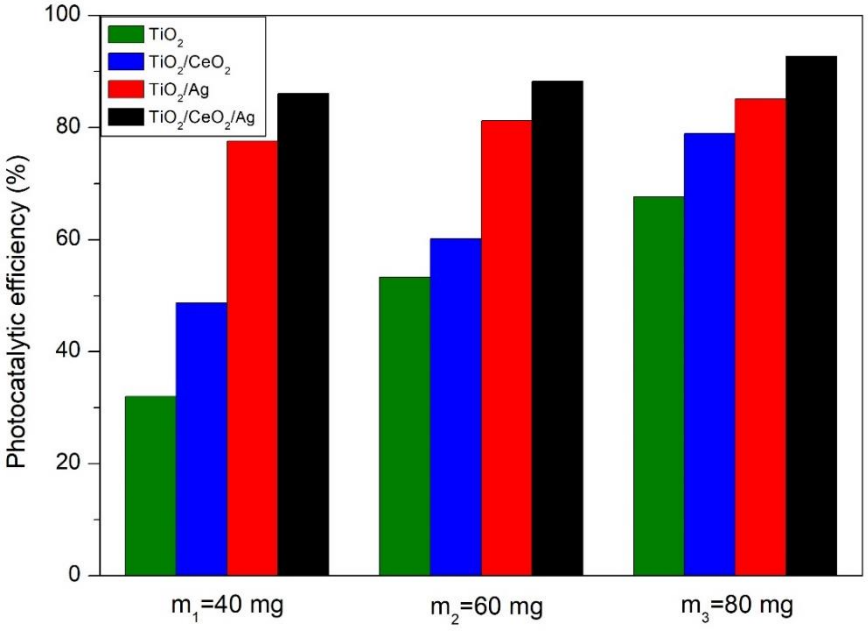

Fig. 9. Effect of catalyst amount using the prepared samples: TiO_2, TiO_2/CeO_2, TiO_2/Ag, and $TiO_2/CeO_2/Ag$ on the photocatalytic efficiency (dye removal in %) of the crystal violet dye

The amount of 80 mg of photocatalyst was selected as the maximum for process optimization, in order to avoid substantial material usage and improve cost-effectiveness. Specifically, near-complete degradation of the CV dye was achieved after 150 min under relatively mild experimental conditions. It was therefore assumed that further increases in catalyst loading would not result in a significant enhancement of photocatalytic efficiency and/or could even lead to a reduction in activity due to the so-called shadow effect.[52,53]

3.5.3. *Effect of irradiation wavelength*

Figure 10 shows the influence of the applied UV wavelengths, $\lambda_1 = 254$ nm and $\lambda_2 = 366$ nm, on the photocatalytic activity of the modified TCA material. All other experimental conditions were kept constant.

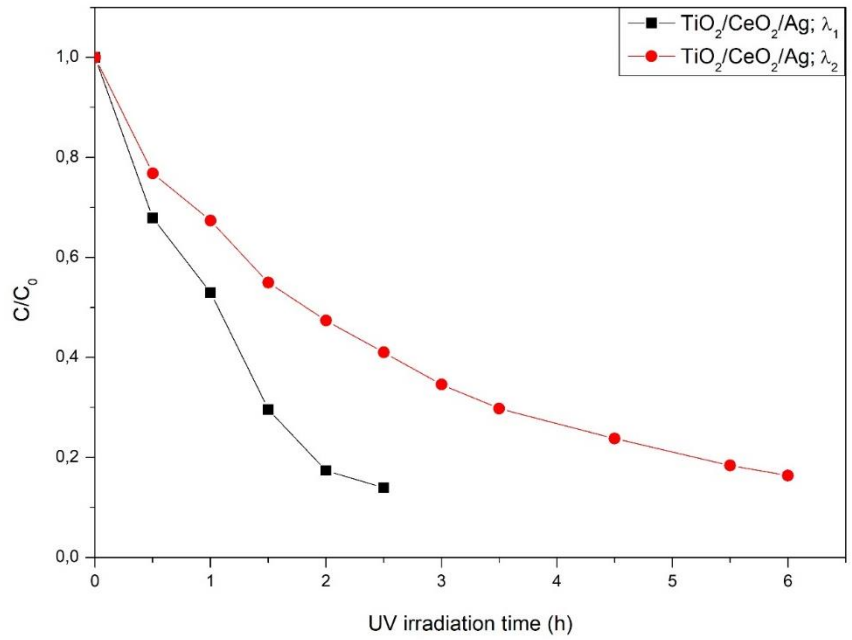

Fig. 10. Effect of irradiation wavelength on the photo-degradation of the crystal violet dye using a $TiO_2/CeO_2/Ag$ catalyst

Based on the presented results (Fig. 10), it was observed that the application of a shorter irradiation wavelength resulted in a significantly faster photocatalytic decomposition. As the wavelength decreased, the photon energy increased, leading to a stronger photon effect and consequently, enhanced photocatalytic efficiency. All samples showed a similar effect after 150 minutes of photocatalytic reaction under the same experimental conditions, as shown in Figure 11.

In Table 3, an overall comparison of the photocatalytic efficiency (crystal violet dye removal in %) after 150 min of UV irradiation for all prepared samples, TiO_2, TiO_2/CeO_2, TiO_2/Ag, and $TiO_2/CeO_2/Ag$, is summarized.

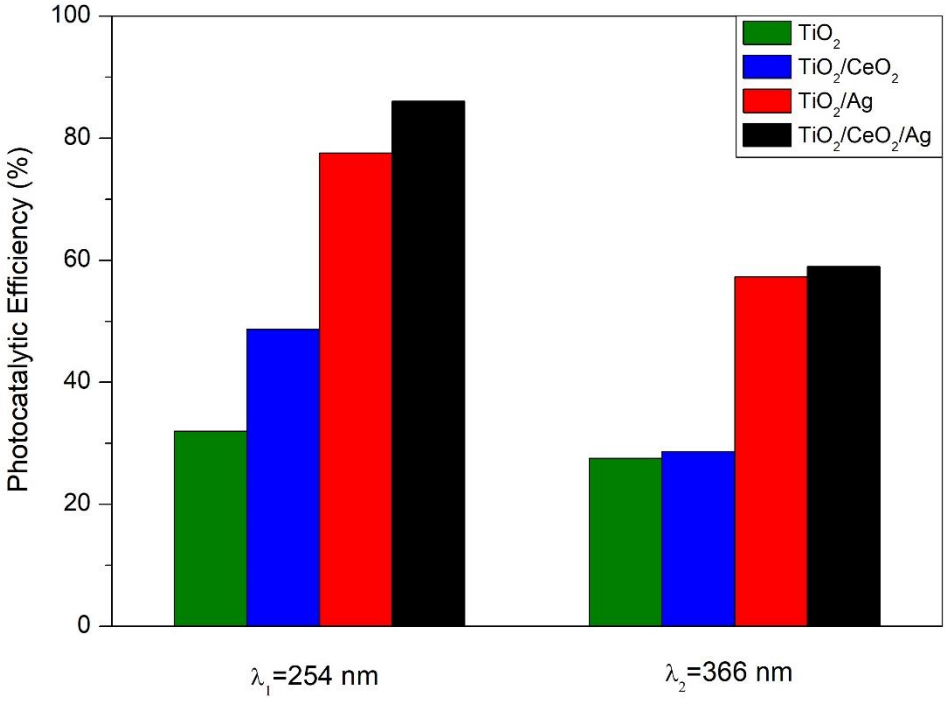

Fig. 11. Effect of irradiation wavelength on the photocatalytic efficiency (dye removal in %) of crystal violet dye using the prepared samples: TiO_2, TiO_2/CeO_2, TiO_2/Ag, and $TiO_2/CeO_2/Ag$

T a b l e 3

Overall comparison of photocatalytic efficiency (dye removal in %) of all prepared catalysts

Process parameters			**Photocatalytic efficiency (dye removal in %) after 150 min of UV irradiation**			
Initial dye concentration (mmol/dm^3)	**Catalyst amount (mg)**	**Irradiation wavelength (nm)**	**TiO_2**	**TiO_2/CeO_2**	**TiO_2/Ag**	**$TiO_2/CeO_2/Ag$**
0.005	40	254	31.99	48.72	77.59	86.07
0.0075	40	254	29.59	33.74	70.55	79.28
0.01	40	254	19.62	21.39	52.94	57.16
0.005	60	254	53.32	60.16	81.23	88.20
0.005	80	254	67.61	78.90	85.06	92.75
0.005	40	366	27.57	28.68	57.31	59.00

4. CONCLUSION

Within the scope of this research, a modified sol–gel synthesis method was used to design and prepare TiO_2, TiO_2/CeO_2, and Ag-doped catalysts (TiO_2/Ag and $TiO_2/CeO_2/Ag$). The obtained results demonstrated enhanced photocatalytic activity of the modified materials, which was attributed to their modified physicochemical properties, including increased specific surface area, restricted crys-

tallite growth, and suppressed anatase-to-rutile phase transformation. All modified catalysts exhibited higher photocatalytic activity compared with pristine TiO_2; TiO_2/CeO_2/Ag showed the best photocatalytic performance.

Notably, the synergistic effect between TiO_2, CeO_2, and Ag significantly enhanced the photocatalytic activity. Specifically, the removal efficiency of the tested CV dye after 150 min of UV irradiation reached approximately 86% when the TiO_2/CeO_2/Ag catalyst was used, whereas only about 32% removal was achieved using pristine TiO_2 under identical experimental conditions. This difference clearly demonstrated the influence of catalyst modification on photocatalytic activity.

Additionally, the optimization of key process parameters during photocatalytic reactions further enhanced photocatalytic efficiency. Overall, these findings encourage further research on the preparation and optimization of modified catalysts, highlighting the important role of doping in improving catalyst efficiency.

Acknowledgements. The work was supported by the Ministry of Science, Technological Development and Innovation of the Republic of Serbia (Numbers: 451-03-136/2025-03/200124, 451-03-137/2025-03/200124, and 451-03-136/2025-03/200051)

REFERENCES

(1) Daghrir, R.; Drogui, P.; Robert D. Modified TiO_2 for environmental photocatalytic applications: a review. *Ind. Eng. Chem. Res.* **2013**, *52*, 3581–3599. https://doi.org/10.1021/ie303468t

(2) Teoh, W. Y.; Scott, J. A.; Amal, R. Progress in heterogeneous photocatalysis: from classical radical chemistry to engineering nanomaterials and solar reactors. *J. Phys. Chem. Lett.* **2012**, *3*, 629–639. https://doi.org/10.1021/jz3000646

(3) Nair, R. R.; Arulraj, J.; Devi, K. R. S. Ceria doped titania nanoparticles: Synthesis and photocatalytic activity. *Mater. Today Proc.* **2016**, *3*, 1643–1649. https://doi.org/10.1016/j.matpr.2016.04.054

(4) Liang, Y.; Ding, H. Mineral-TiO_2 composites: Preparation and application in papermaking, paints and plastics. *J. Alloy. Compd.* **2020**, *844*, 156139. https://doi.org/10.1016/j.jallcom.2020.156139

(5) Chen, X.; Hosseini, S. N.; Van Huis, M. A. Heating-Induced transformation of anatase TiO2 nanorods into rock-salt TiO nanoparticles: Implications for photocatalytic and gas-sensing applications. ACS Appl. Nano Mater. **2022**, *5*, 1600-1606. https://doi.org/10.1021/acsanm.1c04346

(6) Fergus, J. W. Doping and defect association in oxides for use in oxygen sensors. *J. Mater. Sci.* **2003**, *38*, 4259–4270. https://doi.org/10.1023/A:1026318712367

(7) Chen, C.-C.; Chen, W.-C.; Chiou, M.-R.; Chen, S.-W.; Chen, Y. Y.; Fan, H.-J. Degradation of crystal violet by an FeGAC/H_2O_2 procesess. *J. Hazard. Mater.* **2011**, *196*, 420–425. https://doi.org/10.1016/j.jhazmat.2011.09.042

(8) Lee, W.-L. W.; Huang, S.-T.; Chang, J.-L.; Chen, J.-Y.; Cheng, M.-C.; Chen, C.-C. Photodegradation of CV over nanocrystalline bismuth tungstate prepared by hydrothermal synthesis. *J. Mol. Catal. A-Chem.* **2012**, *361–362*, 80–90. https://doi.org/10.1016/j.molcata.2012.04.015

(9) Gao, B.; Lim, T. M.; Subagio, D. P.; Lim, T.-T. Zr-doped TiO_2 for enhanced photocatalytic degradation of bisphenol A. *Appl. Catal. A: Gen.* **2010**, *375*, 107–115. https://doi.org/10.1016/j.apcata.2009.12.025

(10) Vasić, M.; Ranđelović, M.; Momčilović, M.; Matović, B.; Zarubica, A. Degradation of crystal violet over heterogeneous TiO_2-based catalysts: The effect of process parameters. *Process. Appl. Ceram.* **2016**, *10* (3), 189–198. https://doi.org/10.2298/PAC1603189V

(11) Jain, R.; Shrivastava, M. Photocatalytic removal of hazardous dye cyanosine from industrial waste using titanium dioxide. *J. Hazard. Mater.* **2008**, *152*(1), 216–220. https://doi.org/10.1016/j.jhazmat.2007.06.119

(12) Fan, H.-J.; Lu, C.-S.; Lee, W.-L.W.; Chiou, M.-R.; Chen, C.-C.; Mechanistic pathways differences between P25-TiO_2 and Pt-TiO_2 mediated CV photodegradation. *J. Hazard. Mater.* **2011**, *185*(1), 227–235. https://doi.org/10.1016/j.jhazmat.2010.09.022

(13) Krstić, A.; Stanković, H.; Rubežić, M.; Vasić, M.; Zarubica, A. Chemical modifications of nanostructured titania-based materials in photocatalytic decomposition/conversion of various organic pollutants: A short review. *Advanced Technologies*. **2018**, *7*(2), 78–84. DOI: 10.5937/SavTeh1802078K

(14) Navío, J. A.; Colón, G.; Trillas, M.; Peral, J.; Domènech, X.; Testa, J. J.; Padrón, J.; Rodríguez, D.; Litter, M. I. Heterogeneous photocatalytic reactions of nitrite oxidation and Cr(VI) reduction on iron-doped titania prepared by the wet impregnation method. *Appl. Catal. B: Environ.* **1998**, *16*, 187–196. https://doi.org/10.1016/S0926-3373(97)00073-8

(15) Vaithiyanathan, R. Photocatalytic decolourization of reactive dyes using silver incorporated titania catalyst. *Mater. Today Proc.* **2016**, *3*, 4226-4231. https://doi.org/10.1016/j.matpr.2016.11.101

(16) Vaithiyanathan, R.; Sivakumar, T. Studies on photocatalytic activity of the synthesised TiO_2 and Ag/TiO_2 photocatalysts under UV and sunlight irradiations. *Water Sci. Technol.* **2011**, *63*, 377–384. https://doi.org/10.2166/wst.2011.231

(17) Rupa, A. V.; Vaithiyanathan, R.; Sivakumar, T. Noble metal modified titania catalysts in the degradation of Reactive Black 5: A kinetic approach. *Water Sci. Technol.* **2011**, *64*, 1040–1045. https://doi.org/10.2166/wst.2011.524

(18) Rupa, A. V.; Divakar, D.; Sivakumar, T. Titania and noble metals deposited titania catalysts in the photodegradation of tartazine. *Catal. Lett.* **2009**, *132*, 259–267. https://doi.org/10.1007/s10562-009-0108-7

(19) Ivanova, A. S. Physicochemical and catalytic properties of systems based on CeO_2. *Kinet. Catal.* **2009**, *50*, 797–815. https://doi.org/10.1134/S0023158409060020

(20) Li, F. B.; Li, X. Z.; Hou, M. F.; Cheah, K. W.; Choy, W. C. H. Enhanced photocatalytic activity of Ce^{3+}–TiO_2 for 2-mercaptobenzothiazole degradation in aqueous suspension for odour control. *Appl. Catal. A: Gen.* **2005**, *285*, 181–189. https://doi.org/10.1016/j.apcata.2005.02.025

(21) Cano-Casanova, L.; Amorós-Pérez, A.; Lillo-Ródenas, M. Á.; Román-Martínez, M. C. Effect of the preparation method (sol-gel or hydrothermal) and conditions on the TiO_2 properties and activity for propene oxidation. *Materials*. **2018**, *11*, 2227. https://doi.org/10.3390/ma11112227

(22) Wen, B.; Liu, C.; Liu, Y. Optimization of the preparation methods: Synthesis of mesostructured TiO_2 with high photocatalytic activities. *J. Photochem. Photobiol. A Chem.* **2005**, *173*, 7–12. https://doi.org/10.1016/j.jphotochem.2004.12.024

(23) Pulido Melián, E.; González Díaz, O.; Doña Rodríguez, J.M.; Colón, G.; Navío, J.A.; Pérez Peña, J. Effect of hydrothermal treatment on structural and photocatalytic properties of TiO_2 synthesized by sol–gel method. *Appl. Catal. A Gen*. **2012**, *411–412*, 153–159. https://doi.org/10.1016/j.apcata.2011.10.033

(24) Zhu, Q.; Liu, N.; Ma, Q.; Sharma, A.; Nagai, D.; Sun, X.; Zhang, C.; Yang, Y. Sol-gel/hydrothermal two-step synthesis strategy for promoting Ag species–modified TiO_2-based composite activity toward H_2 evolution under solar light, *Mater. Today Energy*. **2021**, *20*, 100648. https://doi.org/10.1016/j.mtener.2021.100648

(25) Nam, C. T.; Yang, W.-D.; Duc, L. M. Solvothermal synthesis of TiO_2 photocatalysts in ketone solvents with low boiling points. *J. Nanomat.* **2013**, *2013*, 627385. http://dx.doi.org/10.1155/2013/627385

(26) Ren, Z.; Zhu, Q.; Cao, L.; Fan, L.; Xu, L.; Xiong, S. Microwave-assisted ultrafast synthesis of TiO_2/MXene/rGO heterojunction electrodes for high-sensitivity electrochemical dopamine detection. *Microchem. J.* **2025**, *218*, 115753. https://doi.org/10.1016/j.microc.2025.115753

(27) Liu, A. R.; Wang, S. M.; Zhao, Y. R.; Zheng, Z. Low-temperature preparation of nanocrystalline TiO_2 photocatalyst with a very large specific surface area. *Mater. Chem. Phys.* **2006**, *99*, 131–134. https://doi.org/10.1016/j.matchemphys.2005.10.003

(28) Elsellami, L.; Dappozze, F.; Fessi, N.; Houas, A.; Guillard, C. Highly photocatalytic activity of nano-crystalline TiO_2 (anatase, rutile) powders prepared from $TiCl_4$ by sol–gel method in aqueous solutions. *Process Saf. Environ*. **2018**, *113*, 109–121. https://doi.org/10.1016/j.psep.2017.09.006

(29) Kim, M. G.; Kang, J. M.; Lee, J. E.; Kim, K. S.; Kim, K. H.; Cho, M.; Lee, S. G. Effects of calcination temperature on the phase composition, photocatalytic degradation, and virucidal activities of TiO_2 nanoparticles. *ACS Omega*. **2021**, *6*, 10668−10678. https://doi.org/10.1021/acsomega.1c00043

(30) Knani, S.; Salhi, R.; Bouzid, M.; Santos, J. M. N.; Selmi, R.; Alenazi, A.; Alenezi, K. A.; Dotto, G. L. Experimental characterization and advanced modeling of the adsorption of Rhodamine B and Crystal Violet on new cobalt metalloporphyrin adsorbent. *Polyhedron*. **2025**, *277*, 117584. https://doi.org/10.1016/j.poly.2025.117584

(31) Koli, V. B.; Kim, J.-S. Photocatalytic oxidation for removal of gases toluene by TiO_2-CeO_2 nanocomposites under UV light irradiation. *Mater. Sci. Semicond. Process.* **2019**, *94*, 70–79. https://doi.org/10.1016/j.mssp.2019.01.032

(32) Hassanzadeh-Tabrizi, S. A. Precise calculation of crystallite size of nanomaterials: A review. *J. Alloys Compd.* **2023**, *968*, 171914. https://doi.org/10.1016/j.jallcom.2023.171914

(33) Aswathappa, S.; Dai, L.; Sathiyadhas, S. J. D.; Kumar, R. S.; Almansour, A. I.; Freire, P. T. C.; Athiruban, S.; Kang, G. Quantitative analysis of anatase-rutile mixtures of TiO_2 employing X-ray diffractometry and visible-Raman spectroscopy at normal heating and superheating conditions. Implications and limitations of the Spurr-Mayers equation, *Ceram. Int.* **2025**, *51* (29), Part B, 61025–61034. https://doi.org/10.1016/j.ceramint.2025.10.297

(34) Spurr, R. A.; Myers, H. Quantitative analysis of anatase-rutile mixtures with an X-ray diffractometer, *Anal. Chem.* **1957**, *29*, 760–762. https://doi.org/10.1021/ac60125a006

(35) Asrafuzzaman, F. N. U.; Amin, K. F.; Gafur, Md. A.; Gulshan, F. Mangifera indica mediated biogenic synthesis of undoped and doped TiO_2 nanoparticles and evaluation of their structural, morphological, and photocatalytic properties. *Results Mater.* **2023**, *17*, 100384. https://doi.org/10.1016/j.rinma.2023.100384

(36) Wang, X.; Xu, H.; Luo, X.; Li, M.; Dai, M.; Chen, Q.; Song, H. Enhanced photocatalytic properties of CeO_2/TiO_2 heterostructures for phenol degradation. *Colloids Interface Sci. Commun.* **2021**, *44*, 100476. https://doi.org/10.1016/j.colcom.2021.100476

(37) Petica, A.; Florea, A.; Gaidau, C.; Balan, D.; Anicai, L. Synthesis and characterization of silver-titania nano-composites prepared by electrochemical method with enhanced photocatalytic characteristics, antifungal and antimicrobial activity. *J. Mater. Res. Technol.* **2019**, *8*(1), 41–53. https://doi.org/10.1016/j.jmrt.2017.09.009

(38) Sangwichien, C.; Aranovich, G. L.; Donohue, M. D. Density functional theory predictions of adsorption isotherms with hysteresis loops. *Colloids Surf. A: Physicochem. Eng. Asp.* **2002**, *206*, 313–320. https://doi.org/10.1016/S0927-7757(02)00048-1

(39) Rouquerol, F., Rouquerol, J., Sing, K., Adsorption by Powders and Porous Solids: Principles, Methodology and Applications; Academic Press. San Diego. **1999**. https://doi.org/10.1016/B978-0-12-598920-6.X5000-3

(40) Thommes, M. Physical adsorption characterization of nanoporous materials. *Chem. Ing. Tech.* **2010**, *82*(7), 1059–1073. https://doi.org/10.1002/cite.201000064

(41) Sing, K. S. W. Reporting physisorption data for gas/solid systems with special reference to the determination of surface area and porosity (Recommendations 1984). *Pure Appl. Chem.* **1985**, *57*(4), 603–619. https://doi.org/10.1351/pac198557040603

(42) Thommes, M.; Kaneko, K.; Neimark, A.V.; Olivier, J.P.; Rodriguez-Reinoso, F.; Rouquerol, J.; Sing, K.S.W. Physisorption of gases, with special reference to the evaluation of surface area and pore size distribution (IUPAC Technical Report). *Pure Appl. Chem.* **2015**, *87*(9–10), 1051–1069. https://doi.org/10.1515/pac-2014-1117

(43) Xu, L.; Zhang, J.; Ding, J.; Liu, T.; Shi, G.; Li, X.; Dang, W.; Cheng, Y.; Guo, R. Pore structure and fractal characteristics of different shale lithofacies in the dalong formation in the western area of the lower yangtze platform. *Minerals*. **2020**, *10*(1) 72. https://doi.org/10.3390/min10010072

(44) Yang, Y.; Zhang, J.; Xu, L.; Li, P.; Liu, Y.; Dang, W. Pore structure and fractal characteristics of deep shale: A case study from permian shanxi formation shale, from the Ordos basin. *ACS Omega*. **2022**, *7*, 9229–9243. https://doi.org/10.1021/acsomega.1c05779

(45) Koli, V.; Dhodamani, A.; More, K.; Acquah, S.F.A.; Panda, D. K.; Pawar, S.; Delekar, S. A simple strategy for the anchoring of anatase titania on multi-walled carbon nanotubes for solar energy harvesting. *Sol. Energy*. **2017**, *149*, 188–194. https://doi.org/10.1016/j.solener.2017.03.036

(46) Li, W.; Liang, R.; Hu, A.; Huang, Z.; Zhou, Y. N. Generation of oxygen vacancies in visible light activated one-dimensional iodine TiO_2 photocatalysts. *RSC Adv*. **2014**, *4*, 36959–36966. https://doi.org/10.1039/C4RA04768K

(47) Wandre, T. M.; Gaikwad, P. N.; Tapase, A. S.; Garadkar, K. M.; Vanalakar, S. A.; Lokhande, P. D.; Sasikala, R.; Hankare, P. P. Sol–gel synthesized TiO_2–CeO_2 nanocomposite: an efficient photocatalyst for degradation of methyl orange under sunlight. *J. Mater. Sci.: Mater. Electron*. **2016**, *27*, 825-833. https://doi.org/10.1007/s10854-015-3823-4

(48) Chen, C.-H.; Shieh, J.; Liao, H.-Y.; Shyue, J.-J. Construction of titania–ceria nanostructured composites with tailored heterojunction for photocurrent enhancement. *J. Eur. Ceram. Soc*. **2014**, *34*, 1523–1535. https://doi.org/10.1016/j.jeurceramsoc.2013.12.019

(49) Ameen, S.; Akhtar, M.S.; Seo, H.-K.; Shin, H.-S. Solution-processed CeO_2/TiO_2 nanocomposite as potent visible light photocatalyst for the degradation of bromophenol dye. *Chem. Eng. J*. **2014**, *247*, 193–198. https://doi.org/10.1016/j.cej.2014.02.104

(50) Vinayagasundaram, C.; Nesaraj, A. S.; Sivaranjana, P. Overview on multicomponent ceramic composite materials used for efficient photocatalysis – An update. *J. Indian Chem. Soc*. **2023**, *100*, 100908. https://doi.org/10.1016/j.jics.2023.100908

(51) Muñoz-Batista, M. J.; Ferrer, M.; Fernández-García, M.; Kubacka, A. Abatement of organics and Escherichia coli using CeO_2-TiO_2 composite oxides: Ultraviolet and visible light performances. *Appl. Catal. B: Environ*. **2014**, *154–155*, 350-359. https://doi.org/10.1016/j.apcatb.2014.02.038

(52) Ma, Y.-S.; Chang, C.-N.; Chiang, Y.-P.; Sung, H.-F.; Chao, A. C. Photocatalytic degradation of lignin using Pt/TiO_2 as the catalyst. *Chemosphere*. **2008**, *71*, 998–1004. https://doi.org/10.1016/j.chemosphere.2007.10.061

(53) Chang, C.-N.; Ma, Y.-S.; Fang, G.-C.; Chao, A. C.; Tsai, M.-C.; Sung, H.-F. Decolorizing of lignin wastewater using the photochemical UV/TiO_2 process. *Chemosphere*. **2004**, *56*, 1011–1017. https://doi.org/10.1016/j.chemosphere.2004.04.021